Chapter 5

Sensitivity of Aerosol Concentrations to the Spatial Distribution of Precipitation

5.1 Introduction

Aerosol particles are relatively short lived in the atmosphere, with typical lifetimes of 1 to 8 days (Andreae 1995). Nevertheless, a growing number of studies are documenting the long-range transport of aerosols thousands of kilometers from their sources (*e.g.*, Clarke et al. 2001; Posfai et al. 1999). Aerosols are known to have several important impacts on the thermodynamic structure of the surface and atmospheric column and their concentrations are expected to grow as a result of industrialization, biomass burning and changes in land-use (Houghton 2001). It is the climate effects of aerosols together with their transport and accumulation in the atmosphere that are causing aerosols to be increasingly viewed as a global environmental concern in addition to a regional air quality problem. This chapter presents a study of aerosol precipitation scavenging, the primary process by which aerosols are removed from the atmosphere. The details of this process, which are poorly constrained by observations, may have important consequences for determining the lifetimes of aerosol particles and their ability to be transported far from their sources.

The direct radiative effect of aerosols is a cooling which results from the scattering of solar energy back to space. Globally, this effect is estimated for the entire column to be in the range of approximately -0.1 to -1.0 W m^{-2} for industrial aerosols and -0.1 to -0.5 W m^{-2} for particles resulting from biomass burning (Houghton 2001). The presence of dark carbonaceous aerosols, however, can lead to a warming of the atmosphere owing to the absorption of sunlight. This observation has led to the conclusion that the column radiative

forcing may, depending on the composition of the aerosol, be the difference between a much stronger surface cooling and atmospheric warming. The Indian Ocean Experiment (INDOEX) determined that the direct radiative influence of black carbon in the wintertime haze layer over the Northern Indian Ocean was an average atmospheric warming of 18 W m^{-2} and surface cooling of -20 W m^{-2} (Ramanathan et al. 2001a). Aerosols are also suspected of modifying the planetary energy budget by increasing the reflectivity of clouds, leading to surface cooling (Twomey 1977), evaporating low clouds, leading to surface heating (Ackerman et al. 2000), suppressing precipitation (Rosenfeld 2000), and perhaps an entire slowing of the hydrological cycle (Ramanathan et al. 2001b). Global values for these indirect aerosol forcing effects remain highly uncertain.

The primary removal process for many aerosol species is scavenging by precipitation. This process occurs both through the nucleation by aerosol particles of cloud droplets that eventually grow large enough to precipitate, as well as the sweep-out of particles below cloud that are impacted by falling droplets (Scott 1978). Quantitative estimates of the scavenging rate are difficult to obtain observationally. Most have been made either through numerical simulation of precipitation and aerosol/cloud microphysics in regional- or global-scale models (where both are highly parameterized), or determined as a residual in large-scale budget estimates. This quantity however is likely to be highly variable and depend strongly on the precipitation regime in the region (*i.e.*, broad stratiform precipitation versus cellular convective precipitation) as well as the proximity of the aerosol source to precipitating clouds.

In addition to aerosol lifetime studies, numerical models are also relied upon for global determinations of climate forcing by aerosols (*e.g.*, Kiehl and Briegleb 1993). Unfortunately, the simulation of precipitation may be biased in coarse models where convection must be parameterized. The frequency distribution of rain rate in satellite observations and a coincident atmospheric simulation using the Model for Atmospheric Transport and

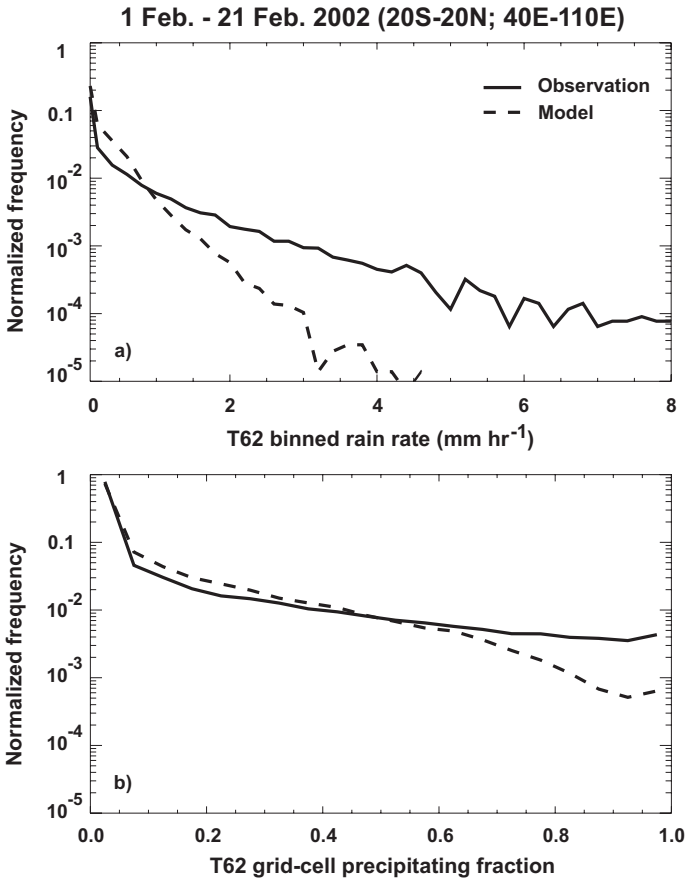

Fig. 5.1. Frequency distributions of (a) rain rate (in mm hr^{-1}), and (b) grid cell precipitating fraction. Solid lines are observations from a multi-platform satellite data set. Dashed lines are simulated rain rates from the MATCH global atmospheric model. All are averages over MATCH grid boxes at T62 resolution.

Chemistry (MATCH) are shown in Fig. 5.1 for precipitation over the Indian Ocean during the winter monsoon. The model is run at the standard T62 resolution (approximately 200 km × 200 km grid cells) and the satellite data have been averaged over the same grid. Extreme precipitation events, some with rain rates exceeding 8 mm hr^{-1}, are evident in satellite observations, while virtually no precipitation greater than 4 mm hr^{-1} is present in the simulation. Furthermore, rain rates greater than 1 mm hr^{-1} occur more frequently in the observations than in the model, while rain rates lower than 1 mm hr^{-1} occur more frequently in the model. The bulk of precipitation in regions of tropical deep convection falls in a relatively few extreme precipitation events. In contrast, simulated precipitation

occurs as broadly distributed gentle precipitation. Wilcox (2002) has argued that this bias results from an absence of fundamental mesoscale convective processes in the convection parameterization of the model.

Because the dynamical structures that produce precipitation are often assumed to be smaller than a model grid cell, another parameter that often enters the numerical simulation of precipitation scavenging is the fraction of the grid cell experiencing rain. Again, the satellite data indicates that this quantity is biased in model simulations. Fig. 5.1b compares the frequency distribution of precipitating fraction in the bottom layer grid cells of the atmospheric model to satellite observations of surface precipitating fraction. The model makes an estimate of the precipitation fraction for each grid cell based on grid cell-averaged value of the production rate of precipitation, as well as the rate of precipitation from above the grid cell, using a parameterization described in section 5.2.2. For comparison, the model grid has been superimposed on the satellite observations and the fractional coverage by observed precipitation of each grid cell is determined. The relative frequency with which grid cells are filled to 60% or less with precipitation is similar in the model and observations. However, precipitating fractions greater than 60% are more frequent in the observations than in the model. While approximately one in every 500 grid cells will be completely filled with precipitation in the observations, only about one in every 5000 will in the model. Low precipitating fractions are consistent with the common assumption that the processes associated with atmospheric convection occur predominantly at scales that are smaller than a grid cell. The observations indicate that a substantial portion of monsoonal precipitation falls in mesoscale precipitation features that exceed the scale of a single model grid cell (Wilcox and Ramanathan 2001).

The purpose of this study is to test the sensitivity of simulated aerosol distributions to the model biases identified above by integrating high-resolution satellite precipitation observations into the MATCH chemical transport model. Separate simulations are per-

formed to test the effects of implementing observed rain rates and observed rain fractions in the scavenging scheme. The model configuration places a tracer source in the surface layer over India to simulate an idealized aerosol. This study compares the horizontal and vertical distributions of aerosol over the Indian Ocean basin using different scavenging criteria. In addition, the role of precipitation in limiting the long-range transport of aerosols beyond the Indian Ocean region is considered.

Aerosols transported off of South Asia during the winter monsoon travel south until they reach the Inter-tropical Convergence Zone (ITCZ). Here the aerosol-laden air masses encounter giant cloud systems containing intense precipitating structures, which provide a potent barrier between the northern and southern hemisphere flows. Despite uncertainties in the estimates of aerosol residence times, the efficiency of precipitation scavenging is evident in data from aircraft flights during INDOEX. A strong gradient was observed in aerosol particle concentrations, from about 1500 cm^{-3} in the Northern Indian Ocean to about 250 cm^{-3} in the Southern Indian Ocean (Ramanathan et al. 2001a).

5.2 Methodology

MATCH is a numerical simulation of the transport of atmospheric constituents based on observed meteorology. The model acquires observed pressure, wind and humidity fields from the NCEP meteorological reanalysis product in order to compute the transport. Precipitation, however, is not provided by the reanalysis data set, therefore MATCH computes precipitation by using standard parameterizations from the NCAR Community Climate Model version 3 (CCM3). Simulated precipitation results from two separately computed processes. Deep convection, which is fully parameterized in the model, is the dominant source of tropical precipitation. Additionally, a small amount of precipitation is produced by stable condensation, which occurs when a grid cell becomes super-saturated. The excess moisture, above saturation, is removed from the grid cell and falls as precipitation. Once the precipitation rate is diagnosed, MATCH computes the scavenging rate by determining the

Table 5.1. Simulation configurations.

name	precipitation source	scavenging parameterization	scavenging computation*
STD	MATCH	MATCH parameterization	Eqns 5.1-5.3
NOSCAV	not applicable	none	
SAT1	satellite	MATCH parameterization	Eqns. 5.1-5.3 $\langle \dot{Q} \rangle$ from satellite
SAT2	satellite	proportional to observed precipitating fraction (no ice phase scavenging)	Eqn. 5.1 F_p from satellite
SAT3	satellite	proportional to observed precipitating fraction (with ice phase scavenging)	Eqn. 5.1 F_p from satellite

* see sections 5.2.2 and 5.2.4.

fraction of aerosol in each grid box to be removed. This depends in large part upon the grid cell precipitation fraction (Balkanski et al. 1993), which is parameterized as a function of the rate of production of precipitating water (see section 5.2.2). To assess the vulnerability of simulated aerosol transport to the representation of precipitation processes in these parameterizations, this study modifies MATCH to receive satellite observations of precipitation at 3 hour intervals.

Comparisons are made of aerosol distributions resulting from five MATCH simulations. The first run (STD) uses the standard configuration of the MATCH model. Precipitation is computed using the parameterizations of convection and stable condensation, and the scavenging rate is computed using the standard parameterization (see section 5.2.2). The second run (NOSCAV) is performed with no precipitation scavenging and establishes an upper bound on the distribution of aerosol. Three separate simulations are performed using satellite observed precipitation. The first (SAT1) tests the sensitivity to the bias in rain rate shown in Fig. 5.1a by replacing model derived rain rates with observed rain rates in the scavenging parameterization. The last two simulations (SAT2 and SAT3) test the precipitating fraction bias apparent in Fig. 5.1b by using the observed precipitating fraction (instead of rain rate) in a new parameterization of scavenging. The satellite-based scavenging

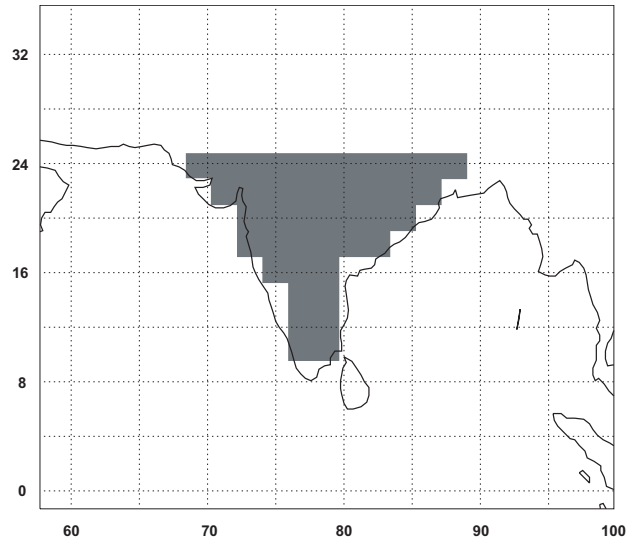

Fig. 5.2. Shaded MATCH grid cells indicate the location of the steady, uniform aerosol source in the bottom layer of the model. Source rate is 2.25 μg m^{-2} s^{-1}.

computation is described in section 5.2.4. The separate model runs are summarized in Table 5.1.

This study focuses on the transport of aerosol from the Indian subcontinent during the winter monsoon. A uniform and steady source of 2.25 μg m^{-2} s^{-1} is applied in the bottom layer of the model over India (see Fig. 5.2 for location of source area). The emissions rate is based on the time- and space-averaged emissions of Rasch et al. (2001) for sulfate, dust and carbonaceous aerosols in South Asia during the INDOEX period. The model is run for 21 days beginning 1 Feb. 2002.

5.2.1 MATCH chemical transport model

MATCH is designed to simulate the sources, sinks and advection of aerosol and trace gas species within the atmosphere. MATCH is an "off-line" transport model, meaning that it is configured to take archived meteorological analysis data sets as input. A description of the data assimilation process, as well as many of the parameterizations used in MATCH can be found in Rasch et al. (1997). The model is run at T62 horizontal resolution (approximately

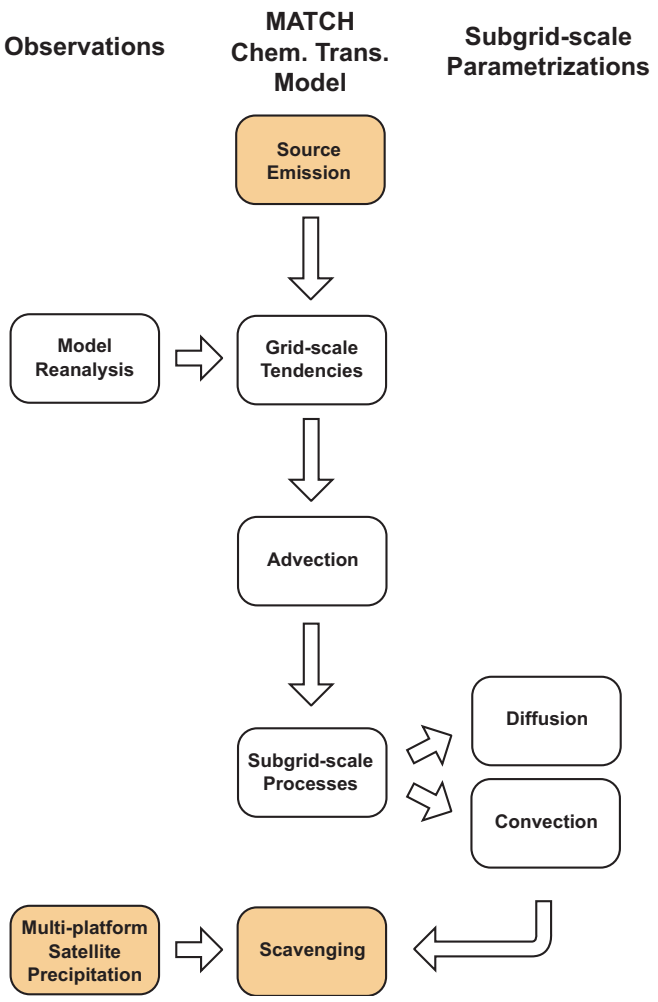

Fig. 5.3. Flow chart for MATCH indicating, in the center column, the key processes acting on simulated aerosol species. Aerosol sources are specified and then advected by grid-scale tendencies determined by the NCEP meteorological reanalysis data set. Advection due to subgrid-scale processes of diffusion and convection are determined by model parameterizations. Experiments are performed here where aerosol removal by precipitation scavenging is determined either by precipitation diagnosed by subgrid-scale parameterizations or observed by satellites. Colored boxes indicate model components that are added or modified in this study. All other components are in the standard MATCH configuration.

200 km × 200 km at the equator) and 28 vertical levels. Some details regarding the convection and scavenging parameterizations are presented below. MATCH has been used for emissions studies (Mahowald et al. 1997a), transport and scavenging of trace gases (Mahowald et al. 1997b; Crutzen and Lawrence 2000), transport of photochemically active species (Lawrence et al. 1999), and transport of tropospheric aerosols (Collins et al. 2001).

A flow chart for MATCH appears in Fig. 5.3. Sources of aerosol are specified and advected by grid-scale tendencies determined by meteorological variables provided by the 3-hourly NCEP/NCAR reanalysis data set (Kalnay et al. 1996). Because significant fluxes of aerosol can result from subgrid-scale contributions to convection and diffusion, additional parameterizations are included in MATCH to compute these tendencies based on the meteorology from the reanalysis product. The deep convection parameterization (Zhang and McFarlane 1995) produces a large portion of the simulated precipitation, particularly in the Tropics. According to the scheme, mass fluxes of a subgrid-scale ensemble of convective updrafts and downdrafts is predicted based on the quantity of convective available potential energy determined from grid cell values of temperature and humidity. Precipitation is produced at a rate that is proportional to the mass flux of the updrafts and a fraction of that precipitation is evaporated in the downdrafts.

Meteorological quantities from the reanalysis data set are provided every 3 hours; however, because of the model resolution and the time scales of subgrid-scale processes, MATCH is operated with a 30-minute time step. Therefore the 3-hourly reanalysis quantities are linearly interpolated to the 30-minute temporal resolution.

5.2.2 Precipitation scavenging parameterization

This section describes the standard MATCH parameterization for precipitation scavenging which is used in the STD and SAT1 simulations. Precipitation scavenging in MATCH is calculated separately for the removal due to the conversion of cloud droplets to precipitating drops within the cloud (in-cloud scavenging), as well as the sweep-out of aerosol by precipitation from above (below-cloud scavenging). In the standard configuration of the model, separate values of precipitation are diagnosed for convection and stable condensation, where stable condensation results from the super-saturation of an entire grid cell. Therefore, for each grid cell there are up to 4 separate scavenging rates, in-cloud and below-cloud scavenging for both convective precipitation and stable condensation. Each of

the four types of scavenging is assumed to be occupying a separate portion of the grid cell, so all four are added together to determine the total aerosol amount scavenged.

The scavenging parameterization is based on the original formulation of Giorgi and Chameides (1986), a simple first-order scheme where the removal rate is proportional to a parameter F_p:

$$\frac{\Delta n}{\Delta t} = \frac{nF_p}{\Delta t} \quad . \tag{5.1}$$

n is the aerosol mass mixing ratio in kg kg^{-1} and Δt is the model time step (30 minutes). Strictly speaking, F_p is the fraction of aerosol in the grid cell that is removed. In the following computation, it is assumed that the aerosol is highly soluble. Under this assumption, all of the aerosol within the cloudy portion of the grid cell is assumed to reside within cloud droplets or precipitating drops. Because highly soluble aerosols are efficiently scavenged by precipitation, F_p is approximately equivalent to the fraction of the grid cell that is precipitating.

Computing F_p begins with determining the fraction of the grid cell occupied by cloud or precipitation, F_{cp}, which is determined in the NCAR CCM3 cloud parameterization scheme (Rasch and Kristjánsson 1998) as the greater of:

$$F_{cp} = \frac{\left\langle F_c \dot{P} \right\rangle_{above}}{\left\langle \dot{P} \right\rangle_{above}} \times \frac{\left\langle \dot{P} - \dot{E} \right\rangle_{above}}{\left\langle \dot{P} \right\rangle_{above}} \qquad \text{or} \qquad F_c \, . \tag{5.2}$$

F_c is the standard cloud fraction from the NCAR CCM3. It is largely based on the relative humidity as in Slingo (1987) and modified as described in Rasch and Kristjánsson (1998). $\dot{P}$ is the production rate of rain water and $\dot{E}$ is the evaporation rate of rain (both in kg m^{-2} s^{-1}). Both are computed with the cloud and convection parameterizations of the model. The $\langle \ \rangle_{above}$ operator denotes the sum over the grid cells above the grid cell at which F_{cp} is being computed.

The precipitating fraction of the grid cell is then estimated as

$$F_p = F_{cp}\frac{\dot{Q}}{L} \tag{5.3}$$

where $\dot{Q}$ is the net production rate of precipitating water and equal to $\dot{P} - \dot{E}$. Also note that the vertically integrated value through the column, $\langle \dot{Q} \rangle$, is equal to the surface rain rate. L is the total condensed water amount in kg m^{-2}.

In the case of precipitation by stable condensation (denoted by subscript *sc*), $\dot{Q}_{sc}$ and L_{sc} are computed by the as part of the Rasch and Kristjánsson (1998) cloud scheme. Therefore they are inserted in to Eqn. 5.3 to compute the precipitating fraction for in-cloud scavenging by stable condensation.

For convective precipitation (denoted by subscript *c*), $\dot{Q}_c$ is computed by the convection parameterization (Zhang and McFarlane 1995), however L_c is not. L_c is therefore assigned the approximate value of 10 kg m^{-2} as in Balkanski et al. (1993). This may be an overestimate and generally ensures that the grid cell precipitating fraction for in-cloud scavenging by convective precipitation is less than 0.1, which is consistent with the assumption that convective precipitation occurs at scales significantly smaller than the model grid cell.

Below-cloud scavenging in nature is determined by the volume swept out by each precipitating drop as it falls from the cloud to the ground (Scott 1978). Lacking a reliable estimate of the number and size of the precipitating drops for either the stable condensation or the convective precipitation, Eqn 5.3 is used for below-cloud scavenging. L is again assigned the value of 10 kg m^{-2} and $\dot{Q}$ is replaced with $\langle \dot{Q}_{sc} \rangle_{above}$ for stable condensation falling from above and $\langle \dot{Q}_c \rangle_{above}$ for convective precipitation from above.

In cloud scavenging is assumed to occur primarily in the liquid phase. At levels between 0^{o}C and -20^{o}C (where liquid and ice are assumed to be mixed) scavenging is reduced by a factor that decreases linearly with temperature from 1 at 0^{o}C to 0 at -20^{o}C. Thus no in-cloud scavenging occurs above the -20^{o}C level. Below cloud scavenging is allowed in the

liquid, ice or mixed phases.

The scavenging scheme described above has been used in a number of models, beginning with that of Giorgi and Chameides (1986), to account for scavenging when details such as the subgrid distribution of precipitation and drop size and number distributions cannot be reliably predicted. It is used here because the goal of the SAT1 experiment is to test a common scavenging scheme where precipitation rate has been replaced with observations, and because it makes an estimate of the grid cell precipitating fraction which can be directly replaced with satellite observations (SAT2 and SAT3 simulations). It is not the purpose of this study to develop a new scavenging scheme for global scale models. According to the scheme, total scavenging is dominated by in-cloud scavenging by stable condensation (Eqn. 5.1). This largely reflects a common assumption that convective precipitation occupies only a small portion of the grid cell it occupies. However, given that most tropical precipitation is produced by the convection parameterization in the model, while known observationally to occur in mesoscale convective structures that can be large enough to fill a single grid cell, the scavenging parameterization likely underestimates scavenging by convective precipitation and overestimates scavenging by stable condensation.

5.2.3 Three-hourly multi-platform satellite precipitation measurements

Precipitation measurements are provided by a blending of measurements from several satellite platforms (Huffman et al. 2001). Complete documentation for the data set is provided by and Huffman and Bolvin (2002), however a few details are described here. Surface rain rate is measured, where available, from each of four passive microwave sensors. Three are Special Sensor Microwave Imagers (SSM/I) mounted on separate Defense Meteorological Satellite Program (DMSP) spacecraft (F13, F14 and F15). DMSP satellites are sun-synchronous polar orbiters with equator crossing times of 5:45, 8:30 and 9:20 respectively. The fourth microwave instrument is the Tropical Rainfall Measuring Mission (TRMM) Microwave Imager (TMI), which has a 46 day precessing orbit with an

equator crossing time that passes through all local hours during the 46 day period. Each microwave instrument is a multi-spectral microwave instrument sensitive to the emission and scattering characteristics of precipitating hydrometeors at wavelengths between 3.5 mm and 2.8 cm. Inversion from microwave brightness temperatures to hydrometeor profiles and surface rain rates is performed using the Goddard Profiling Algorithm (GPROF; Kumerrow et al. 2001). Intercalibration between the microwave instruments is performed whereby all SSM/I retrievals are adjusted by a factor determined by matching the SSM/I retrievals to TMI retrievals where they overlap.

The combined passes of the microwave instruments capture about 40% of the area of the Indian Ocean region during the 21 days of this study. Infrared (IR) estimates of rain rate from geosynchronous satellites are used to fill in the gaps between the microwave measurements. Over the Indian Ocean region, those measurements are provided by the METEOSAT-5 satellite. Precipitation is assigned to all IR pixels with brightness temperature colder than a variable threshold value, which is determined by colocated TMI measurements. The threshold is assigned such that the frequency distribution of 0.25^{o} averaged rain rate in the IR retrieval agrees with the corresponding frequency in the TMI retrievals. The threshold is updated each time step of the precipitation data set using all colocated IR/TMI observations in the region during a 30 day period centered on the time step. The resulting merged microwave/IR data set is provided globally, every three hours beginning 29 Jan. 2002, at 0.25^{o} resolution.

5.2.4 Satellite-based scavenging computation

In the formulation of the scavenging parameterization described in section 5.2.2, the amount of aerosol removed is determined by the grid cell precipitating fraction, F_p, which in turn is determined by the production rate of rain water, $\dot{Q}$. In the SAT1 simulation, the goal is to constrain the computation of F_p in Eqn 5.3 with observed rain rates rather than simulated rain rates. Unfortunately, the precipitation observations only provide a

reliable estimate of the surface rain rate, which is an integral of the production rate of rain water throughout the column above (*i.e.*, $\langle \dot{Q} \rangle$ rather than $\dot{Q}$). This profile of rain production is required by the scavenging parameterization to determine the vertical extent of the scavenging event and the amount removed from each level. Thus a database of MATCH profiles of rain production are taken from the entire 21-day STD simulation and grouped according to surface rain rate. Then a set of 7 average profiles are constructed where all profiles corresponding to rain rates within a factor of 10 in mm hr^{-1} are averaged together. For example, all profiles with MATCH surface rain rates between 10^{-6} and 10^{-5} mm hr^{-1} are averaged together. Likewise, all profiles with rain rates between 10^{-5} and 10^{-4} mm hr^{-1} are averaged together, and so on up to 10 mm hr^{-1}. Scavenging in the SAT1 simulation is performed by applying the profile corresponding to the bin in which the satellite observed surface rain rate falls. Although the sizes of the rain rate bins are broad, the standard deviation of rain production at most levels and most rain rate bins is less than 10%. Therefore, in the SAT1 simulation, scavenging is constrained by observed $\langle \dot{Q} \rangle$.

Scavenging in the SAT2 and SAT3 simulations is computed using Eqn. 5.1, where F_p is the fraction of the surface area at the bottom of the model grid column with non-zero surface rain rate in the satellite data. All aerosol residing within the fraction of the column, F_p, is removed with the constraint that the vertical extent of the scavenging is limited by the vertical extent of rain production in the average profiles described above. In the SAT2 simulation, scavenging is reduced at levels between 0°C and -20°C and does not occur at levels colder than -20°C. In the SAT3 simulation, ice phase scavenging above the freezing level is not restricted. Because all aerosol in the precipitating fraction of the grid cell is scavenged in the SAT3 simulation, it serves as an upper bound on aerosol scavenging. However, by being consistent with Eqn. 5.1, it provides a direct validation of the standard scavenging parameterization by replacing diagnosed values of F with observed values.

Although MATCH has a time step of 30 minutes, the satellite data are only provided

Table 5.2. 21-day averages over Indian Ocean region (30S-30N,40-110E).

	Satellite observations	MATCH (standard model)
precip. (mm day^{-1}), $\langle \overline{\dot{Q}} \rangle$	2.7	4.2
% grid cells containing rain	29	80
% coverage of surface precip., $\overline{F_p}$	7.7	6.8

* overbar denotes time and space averaging.

every three hours. Therefore, the same rain rate values are applied for each 30-minute time step within the 3-hour period. The aerosol is assumed to mix entirely within the grid cell during each 30-minute time step. Thus if a portion of a grid cell is swept clean by precipitation in one time step, aerosol from the remaining portion of the grid cell is made available in the next time step to be swept by the same precipitation feature. This likely results in an overestimation of scavenging, however this assumption is made within all of the simulations compared here, including the STD simulation.

5.3 Simulated and observed precipitation distributions

Fig. 5.1 illustrates an important bias in the model representation of precipitation, specifically that the bulk of simulated precipitation falls as drizzle at the expense of more intense precipitation events. Conversely, as indicated in Table 5.2, the model produces significantly more precipitation than is observed when simulated and observed rain rates are averaged over the entire Indian Ocean basin and 21 day period. The model produces 4.2 mm day^{-1}, while only 2.7 mm day^{-1} is observed. This occurs in spite of the fact that the convection parameterization in the model is constrained by the 3-hourly grid cell-scale reanalysis of meteorological observations. Fig. 5.4 is a comparison of the 21-day mean rain rate over the Indian Ocean basin in MATCH and observed by satellite. The maps clearly indicate that precipitation occurs as more broadly distributed, gentle precipitation in MATCH, with the entire ITCZ region precipitating at an average rate of at least 5 mm day^{-1}. Furthermore, the percentage of grid cells containing precipitation is much higher, by about

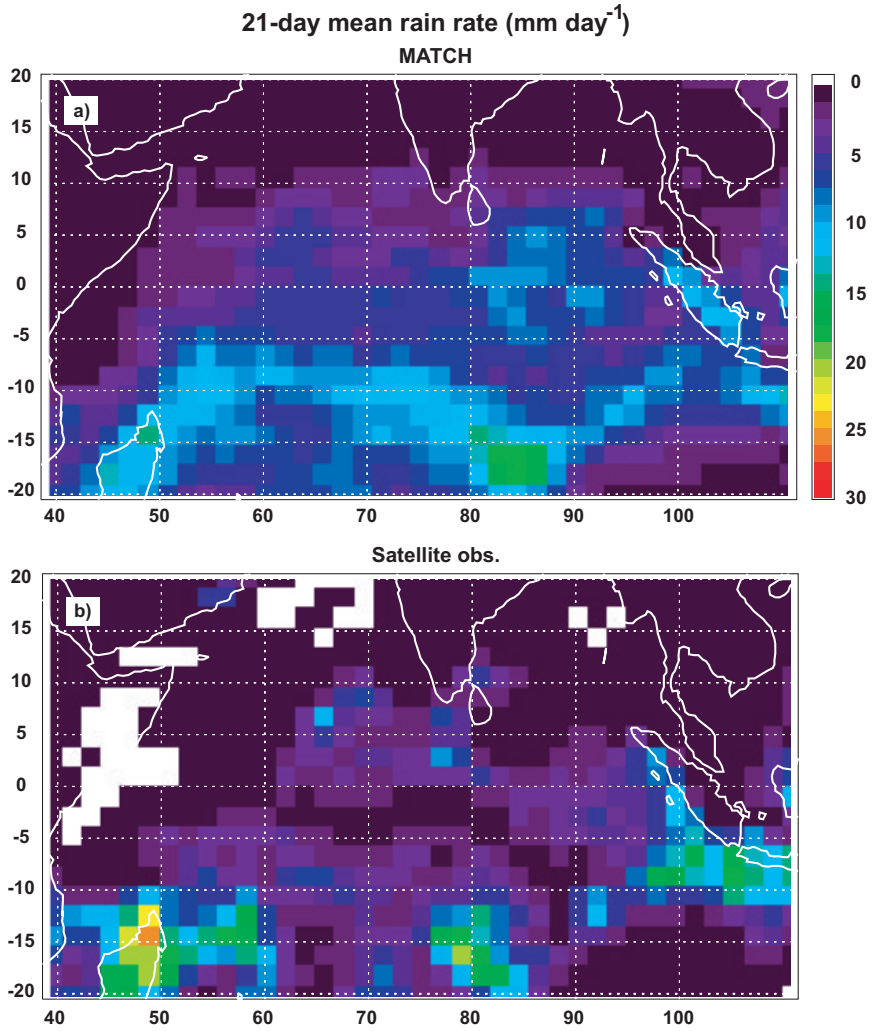

Fig. 5.4. Feb. 1-21, 2002 mean rain rate over the Indian Ocean basin in (a) the MATCH simulation and (b) the satellite observations. Rain rates are in mm day^{-1} and averaged over MATCH grid boxes at T62 resolution.

60%, in MATCH compared to the T62 gridded satellite data, as a result of the broad and steady simulated precipitation. Note that although may more grid cells are precipitating in the model, the scavenging parameterization generally predicts smaller grid cell precipitating fractions (F_p), and the mean precipitating fraction differs from the observed value by only about 1%.

In both the satellite data and the MATCH simulation, precipitation occurs primarily

within a band between 10° S and 20° S latitude, corresponding to the ITCZ typical of the winter monsoon. Three regions of peak precipitation are located over the north coast of Madagascar (50° E), directly south of the tip of India (80° E) and near Indonesia (100° E). Precipitation is stronger at each of these peak regions in the satellite observations by nearly 5 mm day^{-1}. Most other areas have lower mean rain rates in the satellite observations than the MATCH simulation.

5.4 Simulated aerosol distributions

The vertically integrated aerosol distributions after 21 days over the Indian Ocean basin for each of the 5 simulations is shown in Fig. 5.5. Also shown are the values for average aerosol burden over the entire region. The NOSCAV simulation (Fig. 5.5b) puts an upper bound on the aerosol amounts. In the absence of precipitation scavenging, aerosol spreads well south of the equator within 21 days. The average aerosol burden over the region is 31 mg m^{-2}. About 45% of the total aerosol is removed when the standard MATCH scavenging is applied (STD, Fig. 5.5a) and about 40% is removed using the standard MATCH parameterization with observed rain rates (SAT1, Fig. 5.5c). The aerosol burden is reduced by nearly 60%, however, when the fraction of aerosol removed is directly proportional to the observed grid cell fraction of precipitation (SAT2 and SAT3). The slightly higher aerosol amount in the SAT1 simulation relative to the STD simulation indicates there is only a weak dependence of aerosol scavenging on the distribution of rain rates, and may be due to the lower overall amount of precipitation in the satellite measurements. The higher removal rate in the SAT2 and SAT3 simulations indicates a stronger effect for biases in the grid cell fraction of precipitation.

In all simulations with precipitation scavenging, significant aerosol removal occurs within the ITCZ, corresponding with the region of maximum precipitation. ITCZ aerosol removal is most effective in the SAT2 and SAT3 simulations, particularly in the eastern portion of the ITCZ and the region over Indonesia. This may reflect the fact that grid cell

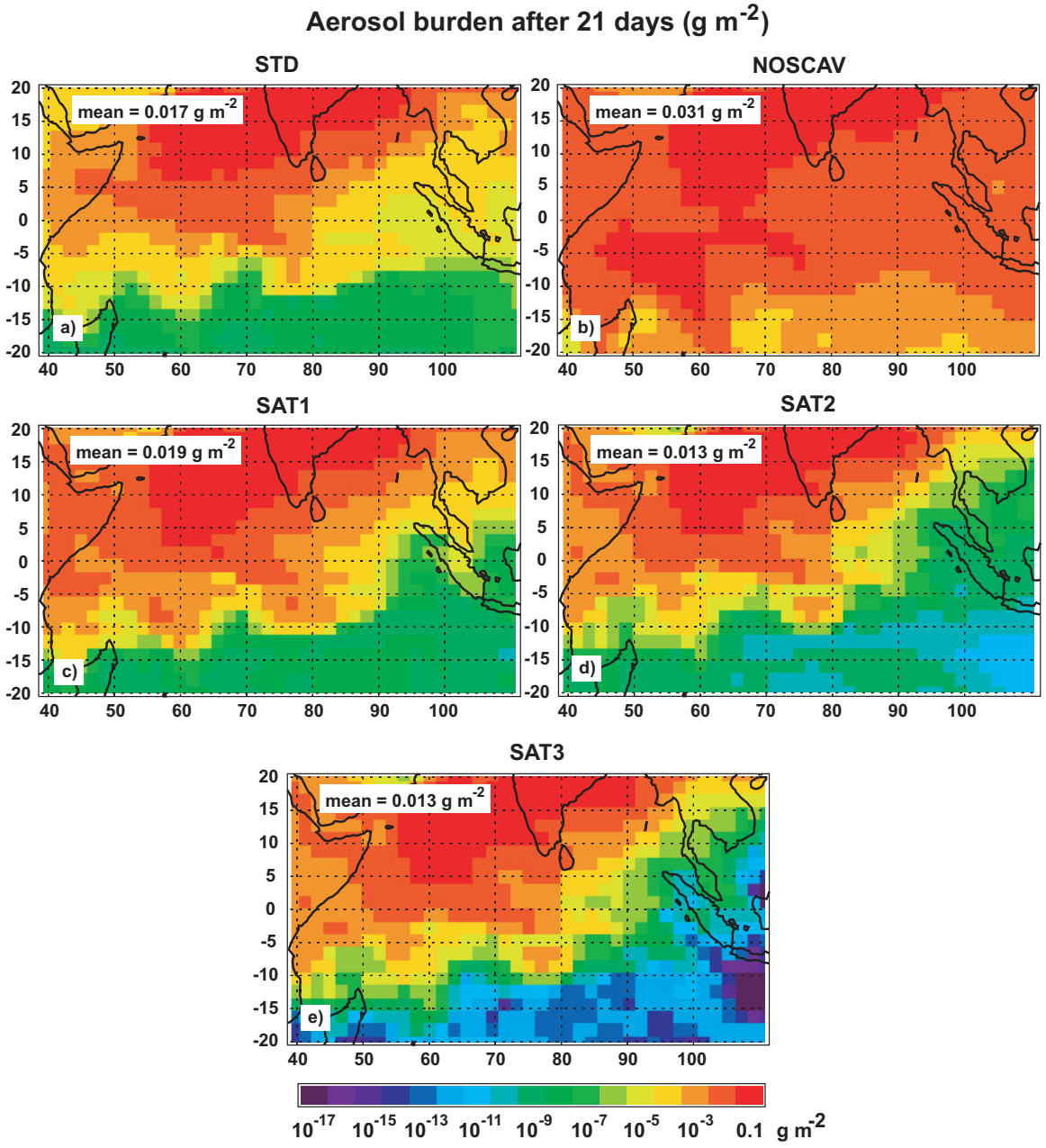

Fig. 5.5. Vertically integrated aerosol burden over the Indian Ocean basin after 21 days in (a) the STD simulation, (b) the NOSCAV simulation, (c) the SAT1 simulations, (d) the SAT2 simulation, and (e) the SAT3 simulation. Units are g m^{-2}.

precipitating fractions greater than 0.8 occur much more frequently in the observations than the model. Such high raining fractions correspond to the more extreme rain rate events that occur along the ITCZ and near Indonesia. Note, however, that even in the STD

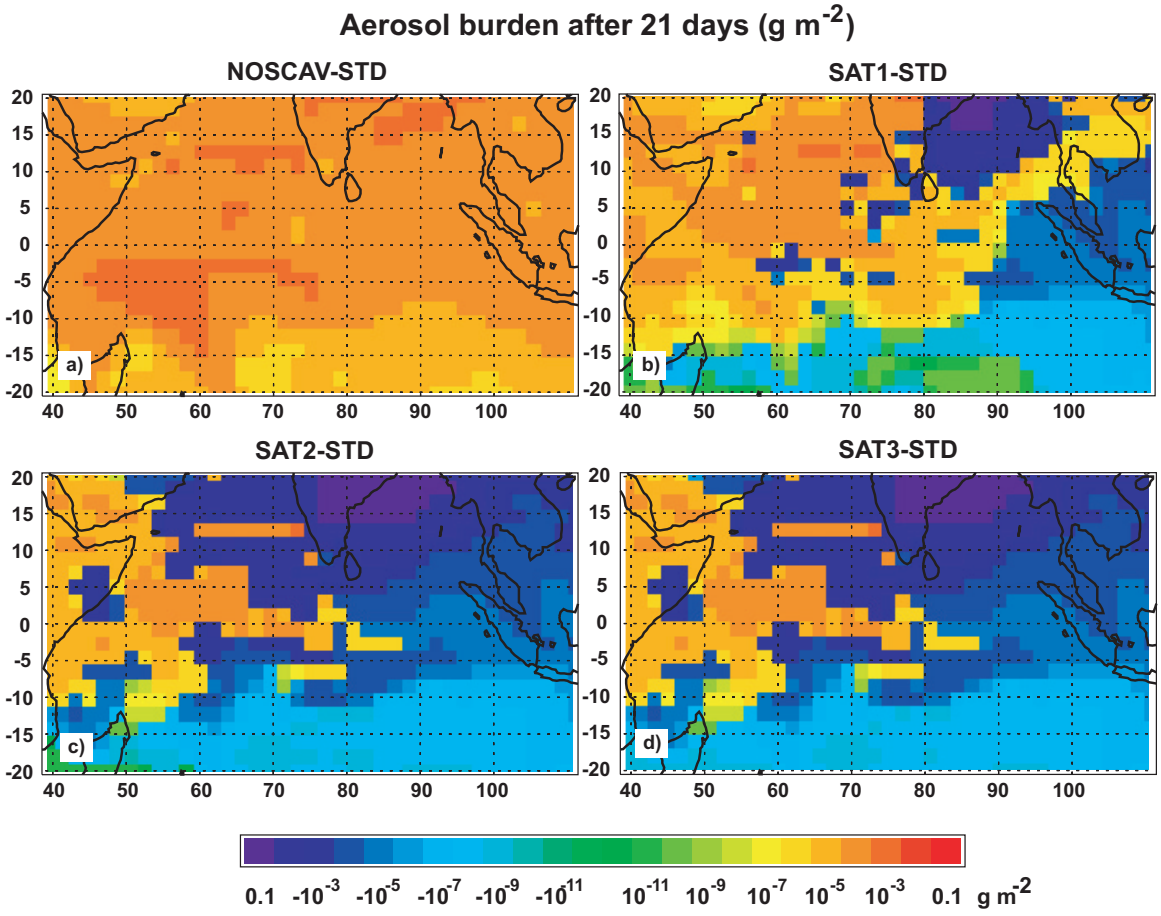

Fig. 5.6. Difference of the vertically integrated aerosol burden over the Indian Ocean basin after 21 days in the STD simulation and (a) the NOSCAV simulation, (b) the SAT1 simulations, (c) the SAT2 simulation, and (d) the SAT3 simulation. Units are g m^{-2}.

and SAT1 simulations, the ITCZ values are several orders of magnitude smaller than in the NOSCAV simulation. Other important differences between the SAT simulations and the STD simulation occur in regions where modest amounts of precipitation occur in the MATCH simulation but none or only trace amounts are observed. These regions have a greater amount of aerosol in the SAT simulations than the STD simulation. This occurs in the western portion of the latitude band between 0° and 10°S as well as the east coast of Africa north of Madagascar. They appear as orange regions in the difference plots shown in Fig. 5.6. An exception to this is the region north of Indonesia, which received less

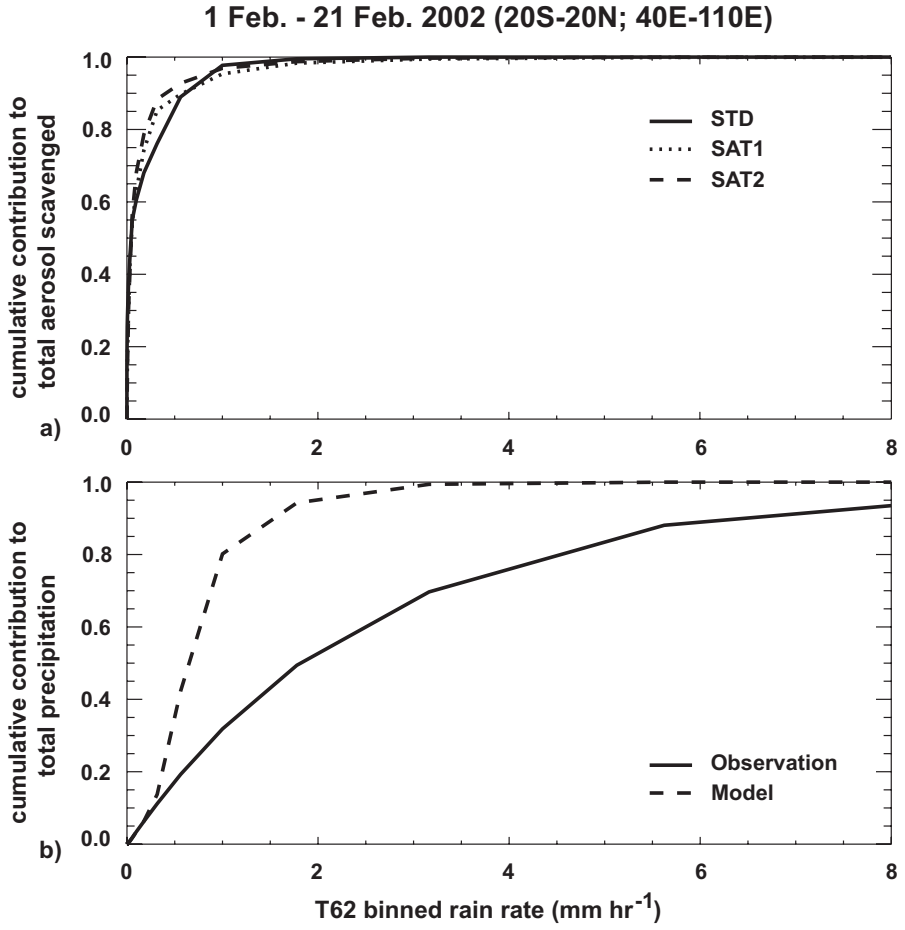

Fig. 5.7. (a) Cumulative contribution to the total aerosol scavenged over the Indian Ocean basin as a function of rain rate. Solid line is STD simulation, dotted line is SAT1 simulation, and dashed line is SAT2 simulation. (b) Cumulative contribution to the total amount of precipitation over the Indian Ocean basin as a function of rain rate. Solid line is satellite observations and dashed line is MATCH model.

precipitation than is simulated by MATCH but has a higher column amount of aerosol in the STD simulation than the SAT2 and SAT3 simulations.

In spite of the differences described above, the aerosol distributions in all of the simulations except for the NOSCAV simulation are similar. In general, the ITCZ represents a significant barrier to the transport of aerosol regardless of how the scavenging is calculated. The cumulative contribution to the total amount of aerosol scavenged is shown in Fig. 5.7a as a function of rain rate for all 5 simulations. For reference, the

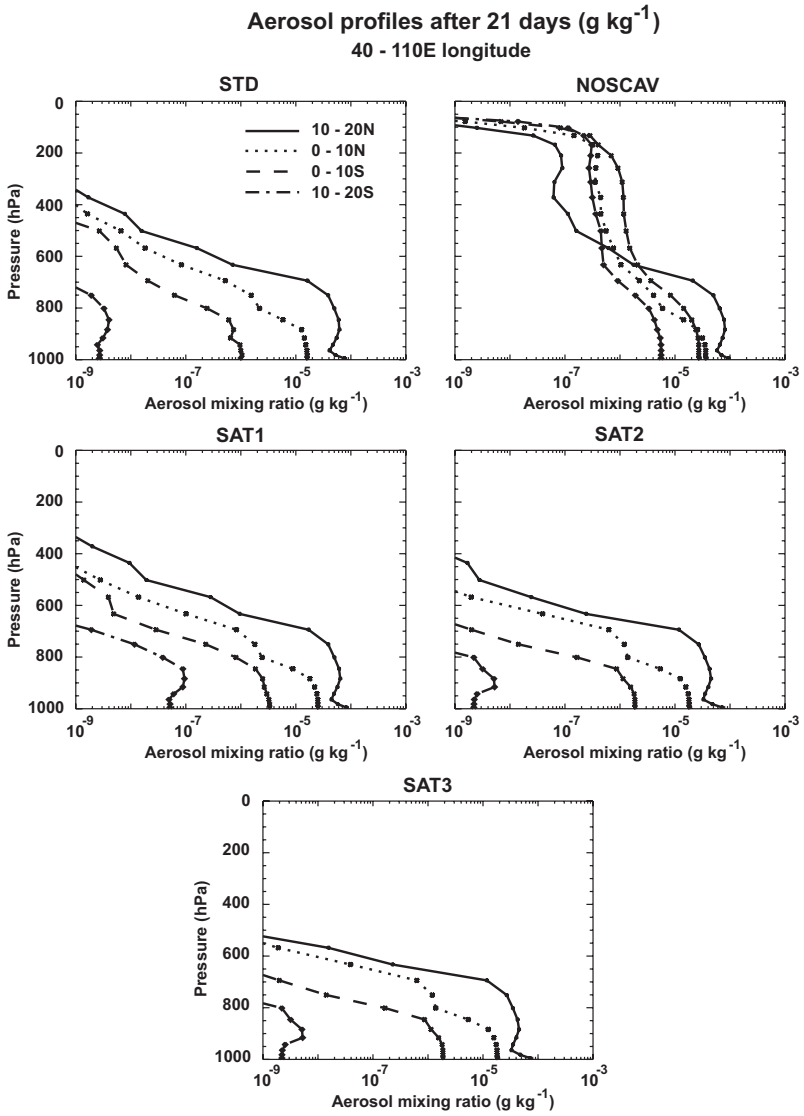

Fig. 5.8. Vertical profiles of aerosol mixing ratio over the Indian Ocean basin in 10^{o} latitude bands for the (a) STD simulation, (b) NOSCAV simulation, (c) SAT1 simulation, (d) SAT2 simulation, and (e) SAT3 simulation. Units are g kg^{-1}.

cumulative contribution to total precipitation as a function of rain rate is shown in Fig. 5.7b. Virtually all scavenging occurs at rain rates less than 1 mm hr^{-1} even while such light rain events account for a relatively small portion of the total amount of precipitation. This may explain why scavenging is not particularly sensitive to the distribution of rain rates. The most important issue is properly determining whether or not precipitation has occurred in

the grid cell.

The vertical distributions of aerosol show a greater sensitivity to biases in the grid cell fraction of precipitation (SAT2 and SAT3) than to biases in rain rate (SAT1). Fig. 5.8 shows vertical profiles of aerosol mixing ratio averaged over 10^{o} latitude bands in the Indian Ocean basin. Without precipitation scavenging, aerosol is allowed to accumulate in the upper troposphere because of vertical transport by convection (Fig. 5.8b). Mixing ratios of 10^{-7} g kg^{-1} or greater are found in every latitude band within a broad layer between 600 hPa and 200 hPa. However, when precipitation scavenging is applied, aerosol transport above 600 hPa is significantly reduced. Differences in the low-level north-south gradient in aerosol amount are also apparent. North of the equator, aerosol amounts below 800 hPa are similar. Between 0^{o} and 10^{o}S, the low-level amount in SAT1 is a factor of 3 larger than the STD simulation and the SAT2 and SAT3 simulations are a factor of 2 larger. Between 10^{o}S and 20^{o}S, the low level amount in SAT1 is more than one order of magnitude larger than the STD simulation. SAT2 and SAT3 boundary layer amounts in this latitude band are only slightly smaller than STD. In the SAT2 and SAT3 simulations, aerosol concentrations above 800 hPa are lower in all latitude bands than in the STD or SAT1 simulations, suggesting that scavenging based on observed precipitating fraction is more effective at scavenging in the middle and upper troposphere. Differences between the SAT2 and SAT3 simulations reflect the effects of ice phase scavenging, and are only apparent above 500 hPa in the 20^{o} - 10^{o}N latitude band. Near the source region, upper-tropospheric aerosol amounts are lower in the SAT3 simulation because of removal by ice. Further north, in the center of the source region, the difference in upper-tropospheric aerosol between SAT2 and SAT3 is more pronounced (not shown).

5.5 Long-range transport of aerosols

There are two primary pathways for aerosol transported beyond the region of the Indian subcontinent and Indian Ocean. The most significant is to the northeast of India

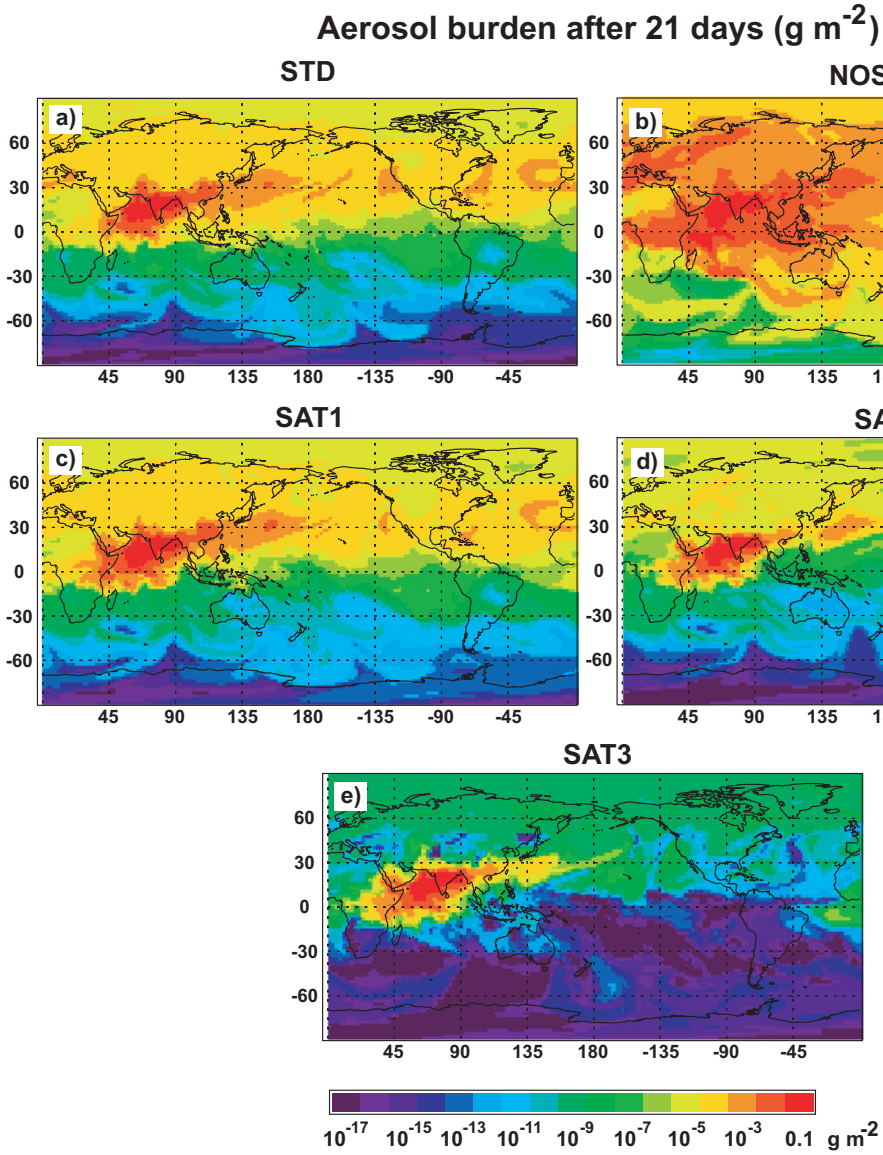

Fig. 5.9. Vertically integrated aerosol burden over the globe after 21 days in (a) the STD simulation, (b) the NOSCAV simulation, (c) the SAT1 simulations, (d) the SAT2 simulation, and (e) the SAT3 simulation. Units are g m^{-2}.

where some of the aerosol gets entrained into the extra-tropical storm track and is efficiently spread throughout the Northern Hemisphere within 21 days. The second is to the Southern Indian Ocean across the ITCZ. Fig. 5.9 shows the global aerosol burden after 21 days for all 5 simulations. In the NOSCAV simulation a broad band of aerosol spreads across the entire Northern Hemisphere extra-tropics. Also a tongue of aerosol laden air crosses the

Table 5.3. Hemispheric-mean aerosol burden after 21-days (mg m^{-2}) excluding Indian Ocean region (20S-20N; 30E-120E).

	Northern Hemisphere	Southern Hemisphere
STD	2.0	0.002
NOSCAV	9.6	1.0
SAT1	1.8	0.004
SAT2	0.8	4.7×10^{-4}
SAT3	0.7	4.5×10^{-4}

ITCZ in the Indian Ocean and eventually enters the Southern Hemisphere storm track to the south of Australia. In the STD simulation, the pathway to the Northern Hemisphere extra-tropics remains important in spite of precipitation scavenging. The pathway across the ITCZ, however is significantly reduced, with the amount of aerosol reaching the Southern Hemisphere reduced by several orders of magnitude compared to the NOSCAV simulation. Table 5.3 shows hemispheric mean aerosol amounts for all simulations, where the Indian Ocean region has been excluded to emphasize the amount transported beyond the region. Southern Hemisphere values are small in all but the NOSCAV simulation. The SAT simulations at least a factor of 2 smaller than the STD simulation in the Southern Hemisphere. Most aerosol that is exported out the region remains in the Northern Hemisphere. Total aerosol in the Northern Hemisphere is 10% smaller in the SAT1 simulation than the STD simulation. Again, with the present scavenging parameterization, there is only weak sensitivity to the distribution of rain rates. The SAT2 and SAT3 simulations have a much more significant effect on total Northern Hemisphere aerosol. Application of satellite observed precipitating fraction reduces Northern Hemisphere aerosol amounts by more than a factor of 2 compared with the STD simulation.

Perhaps the greatest impact on remote aerosol amounts results from the addition of ice phase scavenging. Though the Northern Hemisphere mean values in the Table 5.3 are similar for the SAT2 and SAT3 simulations, these are likely dominated by the values in the

high aerosol tongue extending over China. The stark contrast in Fig. 5.9 between the amount of aerosol in many parts of the Northern Hemisphere in the SAT2 and SAT3 simulations implies that the ability for ice phase precipitation to scavenge aerosol exerts a strong control on the availability of aerosol for transport between continents. In the SAT3 simulation a single tongue of aerosol extends from northern India to the central Pacific Ocean. However, the small amount of aerosol throughout the rest of the Northern Hemisphere suggests that most is removed near the source region prior to reaching the central Pacific Ocean. It should be noted that the significance of low aerosol values, particularly those in the Southern Hemisphere in all of the simulations and the Northern Hemisphere in the SAT3 simulation, cannot be known without additional analysis. For example, in order to assess whether the differences in Southern Hemisphere aerosol amount are significant for radiative forcing, it is necessary to assign radiative properties to the aerosol species, such as scattering and absorption coefficients, which is beyond the scope of this study.

5.6 Summary and conclusion

High resolution, 3-hourly rainfall estimates from multiple satellite platforms has been integrated into the MATCH off-line chemical transport model in order to test the effects of several apparent biases in model simulated precipitation on the concentrations of aerosols in the atmosphere. Errors in the parameterization of tropical deep convection results in a simultaneous over-prediction of total precipitation over the Indian Ocean and a bias toward gently drizzling grid cells at the expense of extreme precipitation events. The effects on aerosol scavenging of biases in simulated rain rates is tested by driving the standard MATCH parameterization of scavenging with grid cell-averaged rain rates from the satellite observations. Simulated scavenging appears to be only weakly effected by changes in the distribution of rain rates. The amount of aerosol scavenged over the Indian Ocean basin is reduced by about 12% when observed rain rates are applied, leading to a slightly higher aerosol burden in the region following a 21 day simulation. This results from a combination

of a 33% lower observed value of 21-day mean rain compared to the MATCH simulation and a substantially fewer number of lightly raining grid cells in the observations. Scavenging at low rain rates dominates the total scavenging and the absence of grid cells with high rain rates in the model does not appear to result in a serious error. When using the MATCH scavenging parameterization, the amount of aerosol removed is much more sensitive to whether or not the model accurately predicts the presence of rain in a grid cell rather than whether the specific rain rate is accurately predicted.

The scavenging parameterization operates by making an estimate of the grid cell fractions containing precipitation. The scavenging rate is directly proportional to the precipitating fraction in the parameterization. Given that there is a rough correlation between surface rain rate and precipitating fraction in the satellite data, the lack of sensitivity to biases in simulated rain rate discussed above suggests that the computation of precipitating fraction is likely flawed. Indeed the parameterized precipitating fraction in the bottom layer of the model is biased toward small precipitating fractions compared to the satellite observations of surface precipitating fraction. The sensitivity of aerosol concentrations to biases in precipitating fraction is tested by replacing the parameterized precipitating fraction with the observed value. Observed precipitation fractions reduce the aerosol amount over the Indian Ocean region by about 24% compared to the STD simulation. Aerosol amounts are less that in the standard model over the entire western portion of the region. The amounts are particularly low in the ITCZ region and south of Indonesia where there is a peak in 21-day mean precipitation and the extreme rain events with high grid cell precipitating fractions occur. Observed precipitation fractions also reduce the vertical extent of the aerosol layer.

Regardless of how aerosol is scavenged, the ITCZ acts as a strong barrier to the transport of aerosol to the Southern Hemisphere. Scavenging based on observed precipitating fraction reduces the total amount of Southern Hemisphere aerosol from 0.002 to 4.7×10^{-4} mg m^{-2} compared to the standard model. Northern Hemisphere aerosol amounts

are reduced by more than a factor to 2 compared to the standard parameterization when observed grid cell precipitating fraction is used in the scavenging. For the remote Northern Hemisphere, aerosol is further reduced with the addition of ice phase scavenging. The aerosol negotiating the pathway to the northeast of the source region toward the Northern Pacific Ocean must reach the upper troposphere in order to accumulate in large amounts over most of the Northern Hemisphere.

References

Ackerman, A. S., O. B. Toon, D. E. Stevens, A. J. Heymsfield, V. Ramanathan, and E. J. Welton, 2000: Reduction of tropical cloudiness by soot. *Science*, **288**, 1042-1047

Andreae, M. O., 1995: Climatic effects of changing atmospheric aerosol levels, in *Future climates of the world: a modeling perspective* (A. Henderson-Sellers, ed.). *World survey of climatology*, **16**, 347-398.

Balkanski, Y. J., D. J. Jacob, G. M. Gardner, W. C. Graustein, and K. K. Turekian, 1993: Transport and residence times of tropospheric aerosols inferred from a global three-dimensional simulation of ^{210}Pb. *J. Geophys. Res.*, **98**, 20,573-20,586.

Clarke, A. D., W. D. Collins, P. J. Rasch, V. N. Kapustin, K. Moore, S. Howell, and H. E. Fuelberg, 2001: Dust and pollution transport on global scales: Aerosol measurements and model predictions. *J. Geophys. Res.*, **106**, 32,555-32,569.

Collins, W. D., P. J. Rasch, B. E. Eaton, B. V. Khattatov, J.-F. Lamarque, and C. S. Zender, 2001: Simulating aerosols using a chemical transport model with assimilation of satellite aerosol retrievals: Methodology for INDOEX. *J. Geophys. Res.*, **106**, 7313-7336.

Crutzen, P. J. and M. G. Lawrence, 2000: The impact of precipitation scavenging on the transport of trace gases: A 3-dimensional model sensitivity study. *J. Atmos. Chem.*, **37**, 81-112.

Giorgi, F. and W. L. Chameides, 1986: Rainout lifetimes of highly soluble aerosols and gases as inferred from simulations with a general circulation model. *J. Geophys. Res.*, **91**, 14 367-14 376.

Houghton, J. T., Y. Ding, D. J. Griggs, M. Noguer, P. J. van der Linden, and D. Xiaosu, Eds., 2001: *Climate Change 2001: The Scientific Basis: Contribution of Working Group 1 to the Third Assessment Report of the Intergovernmental Panel on Climate Change*. Cambridge University Press, 944 pp.

Huffman, G. J., R. F. Adler, D. T. Bolvin, E. J. Nelkin, and E. F. Stocker, 2001: A New Fine-Scale, Quasi-Global Combined Precipitation Estimate Based on TRMM, *Proc. of the 11th Am. Meteoro. Soc. Conf. On Satellite Meteorology and Oceanography,* Madison, Wisconsin.

Huffman, G. J. and D. T. Bolvin, 2002: TRMM real-time multi-satellite data set documentation. Unpublished manuscript avail. from ftp://agnes.gsfc.nasa.gov/pub/huffman/rt_examples/docs/3B4XRT_doc.

Kalnay, E. and co-authors, 1996: The NCEP/NCAR 40-year reanalysis project. *Bull. Am. Meteorol. Soc.*, **77**, 437-471.

Kiehl, J. T. and B. P. Briegleb, 1993: The relative roles of sulfate aerosols and greenhouse gases in climate forcing. *Science*, **260**, 311-314.

Kummerow, C., Y. Hong, W. S. Olson, S. Yang, R. F. Adler, J. McCullum, R. Ferraro, G. Petty, D. -B. Shin and T. T. Wilheit, 2001: The evolution of the Goddard Profiling Algorithm (GPROF) for rainfall estimation from passive microwave sensors. *J. Appl. Meteor.*, **40**, 1801-1820.

Lawrence, M. G., P. J. Crutzen, P. J. Rasch, B. E. Eaton and N. M. Mahowald: A model for studies of tropospheric photochemistry: Description, global distributions, and evaluation. *J. Geophys. Res.*, **104**, 26 245-26 277.

Mahowald, N. M., R. G. Prinn and P. J. Rasch, 1997a: Deducing CCl_3F emissions using an inverse method and chemical transport models with assimilated winds. *J. Geophys. Res.*, **102**, 28 153-28 168.

Mahowald, N. M., P. J. Rasch, B. E. Eaton, S. Whittlestone and R. G. Prinn, 1997b: Transport of ^{222}Radon to the remote troposphere using MATCH and assimilated winds from ECMWF and NCEP/NCAR. *J. Geophys. Res.*, **102**, 28 139-28 151.

Posfai, M., J. R. Anderson, P. R. Buseck, and H. Sievering, 1999: Soot and sulfate aerosol particles in the remote marine troposphere. *J. Geophys. Res.*, **104**, 21,685-21,693.

Ramanathan, V. and co-authors, 2001a: Indian Ocean Experiment: An integrated analysis of the climate forcing and effects of the great Indo-Asian haze. *J. Geophys. Res.*, **106**, 28,371-28-398.

Ramanthan, V., P. J. Crutzen, J. T. Kiehl, and D. Rosenfeld, 2001b: Aerosols, Climate and the Hydrological Cycle. *Science*, **294**, 2119-2124.

Rasch, P. J., N. M. Mahowald, and B. E. Eaton, 1997: Representations of transport, convection, and the hydrological cycle in chemical transport models: Implications for the modeling of short-lived and soluble species. *J. Geophys. Res.*, **102**, 28 127-28 138.

Rasch, P. J., and J. E. Kristjánsson, 1998: A comparison of the CCM3 model climate using diagnosed and predicted condensate parameterizations. *J. Climate*, **11**, 1587-1614.

Rasch, P. J., W. D. Collins, and B. E. Eaton, 2001: Understanding the Indian Ocean Experiment (INDOEX) aerosol distributions with an aerosol assimilation. *J. Geophys. Res.*, **106**, 7337-7355.

Rosenfeld, D., 2000: Suppression of rain and snow by urban and industrial air pollution. *Science*, **287**, 1793-1796.

Scott, B. C., 1978: Parameterization of sulfate removal by precipitation. *J. Appl. Meteor.*, **17**, 1375-1389.

Slingo, J. M. 1987: The development and verification of a cloud prediction scheme for the ECMWF model. *Quart. J. Roy. Meteor. Soc.,* **113**, 899-927.

Twomey, S., 1977: The influence of pollution on the shortwave albedo of clouds. *J. Atmos. Sci.*, **34**, 1149-1152.

Wilcox, E. M. and V. Ramanathan, 2001: Scale dependence of the thermodynamic forcing of tropical monsoon clouds: Results from TRMM observations. *J. Climate*, **14**, 1511-1524..

Wilcox, E. M., 2002: Spatial and temporal scales of precipitating tropical cloud systems in satellite imagery and the NCAR CCM3. *J. Climate*, accepted pending revision.

Zhang, G. J. and N. A. McFarlane, 1995: Sensitivity of climate simulations to the parameterization of cumulus convection in the Canadian Climate Centre General Circulation Model. *Atmos.-Ocean*, **33**, 407-446.